RAA 2016 Vol. **16** No. **10**, 159 (12pp) doi: 10.1088/1674–4527/16/10/159
http://www.raa-journal.org *http://iopscience.iop.org/raa*

***R**esearch in*
***A**stronomy and*
***A**strophysics*

Spectral indices for radio emission of 228 pulsars

Jun Han[1,2], Chen Wang[1], Jun Xu[1] and Jin-Lin Han[1]

[1] National Astronomical Observatories, Chinese Academy of Sciences, Beijing 100012, China; *hanjun@nao.cas.cn*
[2] School of Astronomy, University of Chinese Academy of Sciences, Beijing 100049, China

Received 2016 April 17; accepted 2016 April 21

Abstract We determine spectral indices of 228 pulsars by using Parkes pulsar data observed at 1.4 GHz, among which 200 spectra are newly determined. The indices are distributed in the range from -4.84 to -0.46. Together with known pulsar spectra from literature, we tried to find clues to the pulsar emission process. The weak correlations between the spectral index, the spin-down energy loss rate $\dot{E}$ and the potential drop in the polar gap $\Delta\Psi$ hint that emission properties are related to the particle acceleration process in a pulsar's magnetosphere.

Key words: pulsars: general — radiation mechanisms: general — radio continuum: general

1 INTRODUCTION

The pulsar emission mechanism has been a long standing problem since the discovery of the first pulsar in 1968 (Hewish et al. 1968). There has been much effort to understand emission properties in both observational and theoretical aspects. Based on observations, cone and core components, which have different spectral indices and polarization properties, have been identified from mean pulsar profiles (Rankin 1983). Theoretically, it is not yet clear whether the emission is generated above the polar cap or near the light cylinder, though radio polarization angle curves hint at the region near the polar cap (Radhakrishnan & Cooke 1969; Komesaroff 1970), while multi-band observations of the Crab pulsar show that the emission comes from the very outer region near the light cylinder in the pulsar magnetosphere (Moffett & Hankins 1996). The very steep spectra and very high temperature of pulsar emission are very intriguing, and imply that the emission is generated by a bunch of particles in a coherent mode (Melrose 2006) when they drift out in a pulsar magnetosphere. Because of scintillation due to motion of irregular clumps in the interstellar medium, the radio flux densities of point sources such as nearby pulsars are difficult to measure, especially at low frequencies. Previously, flux densities of pulsars had to be measured at many epochs at several frequencies, and then were averaged and fitted for spectral indexes to overcome different scintillations at different frequencies.

The flux density measurements S_ν observed at a number of frequencies ν are fitted by a power law, $S_\nu \sim \nu^\alpha$, to get a spectral index, α. Pulsar spectral indices have previously been determined from measurements in wide frequency ranges (see Table 1). Sieber (1973) made the first extensive analysis of spectra of 27 pulsars observed with the German 100 m and 25 m telescopes along with flux densities published in literature, and found the turnover behavior at low frequencies and spectral break at high frequencies. Malofeev et al. (1994) published spectra for 45 pulsars by using flux densities over a wide frequency range from 0.1 GHz to 30 GHz. A comprehensive database for pulsar flux densities of 280 pulsars from 0.4 GHz to 1.6 GHz was published by Lorimer et al. (1995). They found a weak inverse correlation between spectral index and characteristic age for normal pulsars and a strong positive correlation between spectral index and period for millisecond pulsars. Toscano et al. (1998) published flux densities for 216 southern pulsars and 19 millisecond pulsars between 436 MHz and 1660 MHz and showed that normal pulsars have a spectral index between -3.5 and $+0.5$ with a peak around -1.7, while millisecond pulsars have spectral indices in a narrow range between -3 and -1. Kramer et al. (1998) also analyzed spectra of 23 millisecond pulsars and found that the indices are distributed in the range from -1.0 to -2.0, which is much narrower than the range for normal pulsars. Kijak et al. (1998) analyzed pulse shape at 4.85 GHz and determined spectral indices from flux densities at 1.4 GHz and 4.85 GHz for 144 weak pulsars, and showed the spectral index distribution peaks around -1.8 in the range $-3.7 \sim -0.3$. Maron et al. (2000) collected flux densities between 0.4 GHz and 23 GHz in literature and analyzed spectra for 281 pulsars, and found that some pulsars have a spectral break near 1 GHz or lower frequencies, which are probably due to some components disappearing at high frequencies as noticed previously (Sieber et al. 1975; Izvekova et al. 1979; Kramer et al. 1999).

In this paper, we present new measurements for flux densities of 228 pulsars at the four subbands within a to-

Table 1 Pulsar Spectral Analyses and Frequency Ranges

Reference	Number	Frequency (GHz)
Sieber (1973)	27	$0.1 \sim 10$
Malofeev et al. (1994)	20	$0.1 \sim 30$
Lorimer et al. (1995)	280	$0.4 \sim 1.6$
Malofeev et al. (1996)	284	$0.1 \sim 10$
Toscano et al. (1998)	216	$0.4 \sim 1.6$
Kijak et al. (1998)	144	$1.4 \sim 4.9$
Maron et al. (2000)	266	$0.4 \sim 23$
This paper	228	$1.2 \sim 1.5$

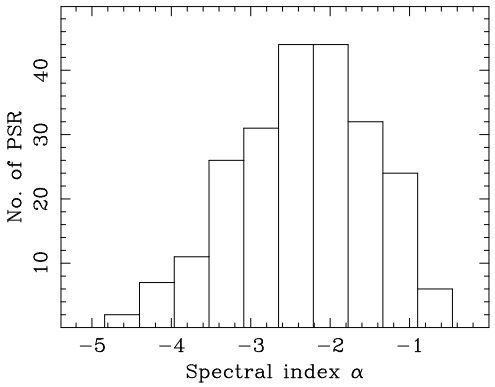

Fig. 1 Distribution of spectral indices for the 228 pulsars peaks at around -2.2 in the range from -4.8 to -0.5.

tal bandwidth of 256 MHz around 1.4 GHz observed with the Parkes 64 m telescope, from which spectral indices are determined.

In Section 2, we describe our observations and data reduction procedures. In Section 3, our results are compared with data in the literature, and the spectral indices are correlated with pulsar characteristic parameters to seek any hint on the emission process. The conclusions are given in Section 4.

2 OBSERVATIONS AND DATA REDUCTION

About 500 pulsars have been observed with the Parkes telescope between August 2006 and February 2008. Data were taken by using the central beam of the multibeam receiver at a central frequency of 1369 MHz and a bandwidth of 256 MHz, with one exceptional session in March 2007 in which the H-OH receiver was used to observe at a central frequency of 1433 MHz. These observations were all well calibrated with the on and off observations of the strong radio source Hydra A, which has a flux density of 43 Jy at 1400 MHz. All data were folded online to produce mean pulse profiles in every 1-minute sub-integrations for 512 frequency channels.

In the offline data reduction, we cleaned the radio frequency interference in a channel-time data cube by removing some bad channels and some strong term interference in the wide band. We then obtained the mean pulsar profiles in four subbands by summing data of all sub-integrations and two polarizations, and measured the pulsar mean flux densities at these four subbands, as listed in Table 2. The uncertainty of the mean flux density was estimated from the standard deviation of the off-pulse window and the sampling number of the on-pulse window.

To derive the spectral index, we applied a weighted least-squares approach by fitting a power law to the mean flux densities at these four subbands, and calculated the standard error σ_α of α by the χ^2 minimization technique. We found that most pulsars either scintillate or are too weak in some or all subbands, which means that we cannot properly fit the spectral index. Only when the pulsar dispersion measure DM $\gtrsim 100\,\mathrm{cm}^{-3}$ pc and pulsars are strong enough can the scintillation effect be averaged out. The spectral indices we obtained are distributed in the range from -4.8 to -0.5, with a peak around -2.2, as shown in Figure 1.

3 RESULTS AND DISCUSSIONS

We calculated the flux densities of 228 pulsars at four subbands which can be consistently fitted with a power law, as listed in Table 2. Note that previously, pulsars were observed for getting spectral indices using different telescopes by different authors, and/or calibrated by different sources or processed with different procedures, which may introduce different systematic uncertainties. Our measurements presented here are carried out in a relatively smaller frequency range, and the flux densities are measured by one set of instruments in one wide band observation and are consistently calibrated by one source with the same procedure, which can avoid not only systematic uncertainties but also pulsar flux density changes due to long-term deflective or reflective scintillation effects. The flux densities of these pulsars at four subbands are fitted with a power law to get the spectral indices as shown in Figure 2.

We also compiled the spectral indices of pulsars in the literature. Previously, spectral indices have been determined for 426 pulsars (Sieber 1973; Kramer et al. 1998; Malofeev et al. 1994; Lorimer et al. 1995; Toscano et al. 1998; Kijak et al. 1998; Maron et al. 2000; Sieber et al. 1975; Izvekova et al. 1979; Kramer et al. 1999; Cordes 1978; Dembska et al. 2014; Bates et al. 2011; Slee et al. 1986; Deneva et al. 2009; Foster et al. 1991; Hobbs et al. 2011; Joshi et al. 2009; Lambert & Rickett 1999; Lommen et al. 2000; Lorimer & Xilouris 2000; McLaughlin et al. 2002; Malofeev 1996; Malofeev et al. 2000; Rankin et al. 1970; Robinson et al. 1968). In our sample, 28 pulsars have their spectral indices determined in the literature, and 200 weak pulsars have newly determined spectral indices. We compared the spectral indices of 28 pulsars we measured with those in literature in Table 3, and found that our values are systematically steeper. Our results probably seem to be reasonable because the frequency range for flux densities we measured is at the high end of the wide multi-frequency range in literature and because flux densities at lower frequencies always show a turn-over which causes a global flat spectrum.

To find clues on the pulsar emission process, in Figure 3 we plot the spectral indices of pulsars against

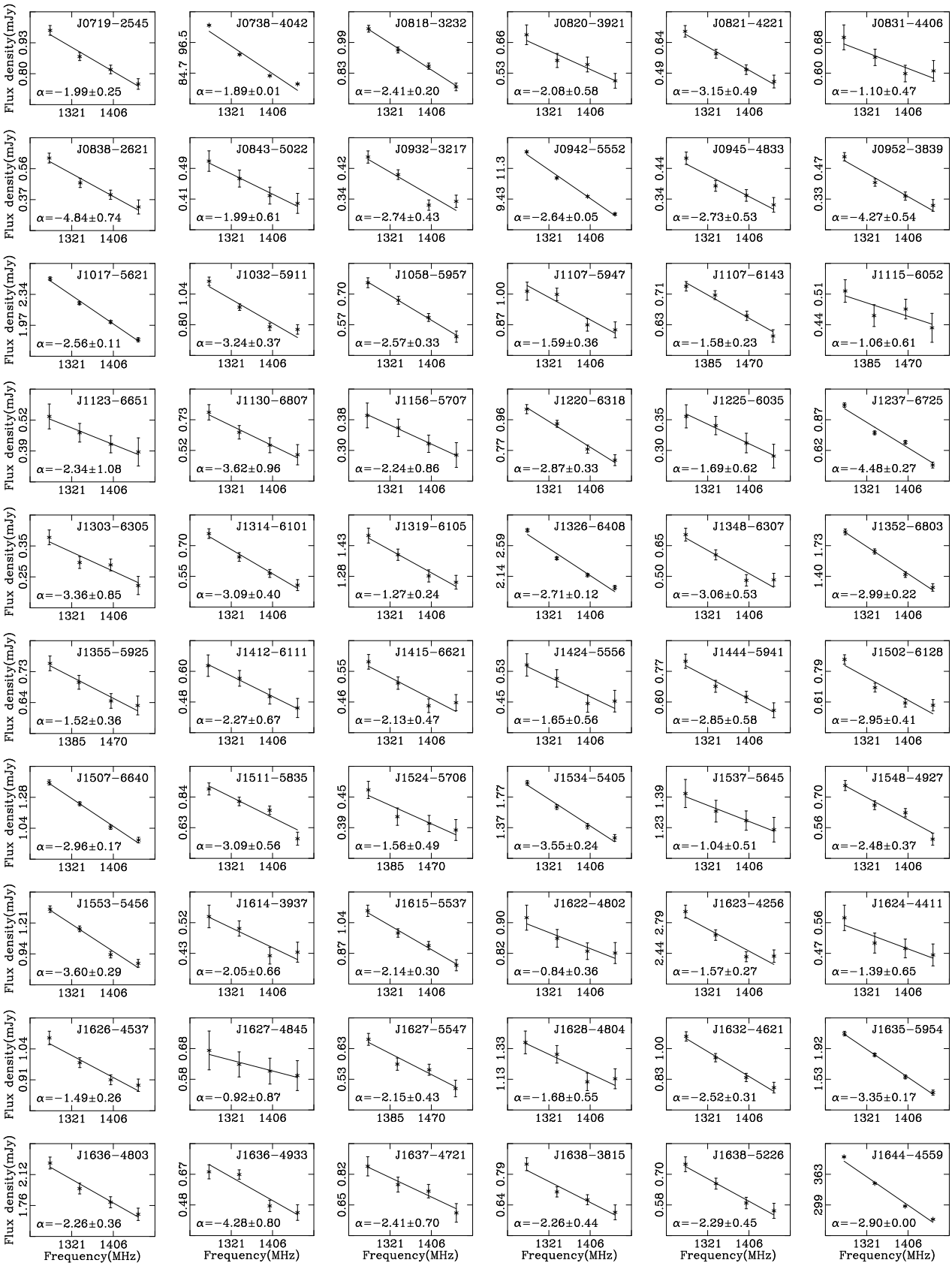

Fig. 2 The flux densities at four subbands are fitted for spectral indices of 228 pulsars. Both the X-axis for the frequency and Y-axis for the flux density are plotted on a logarithmic scale. These plots are continued in the following pages.

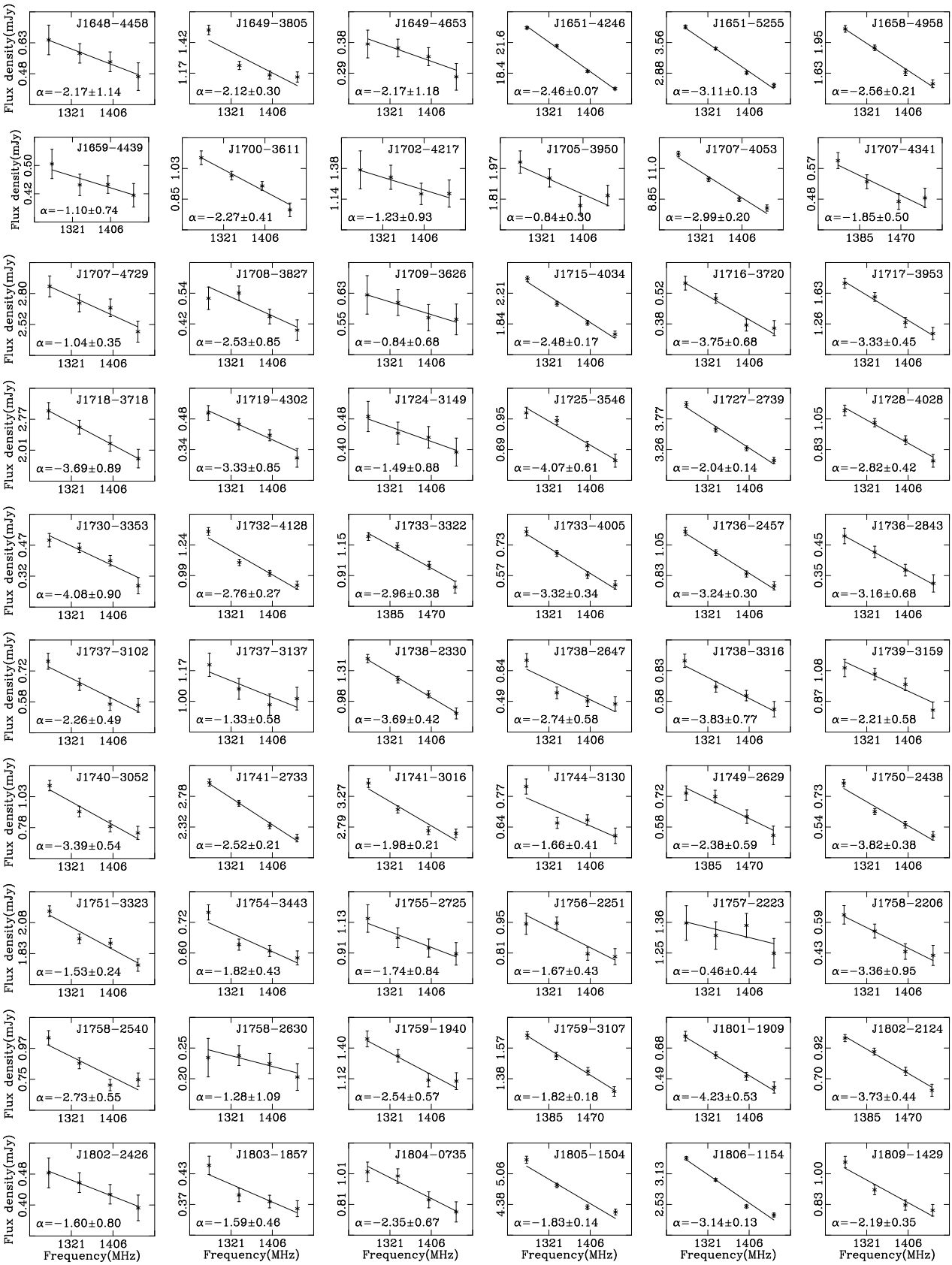

Fig. 2 — *Continued.*

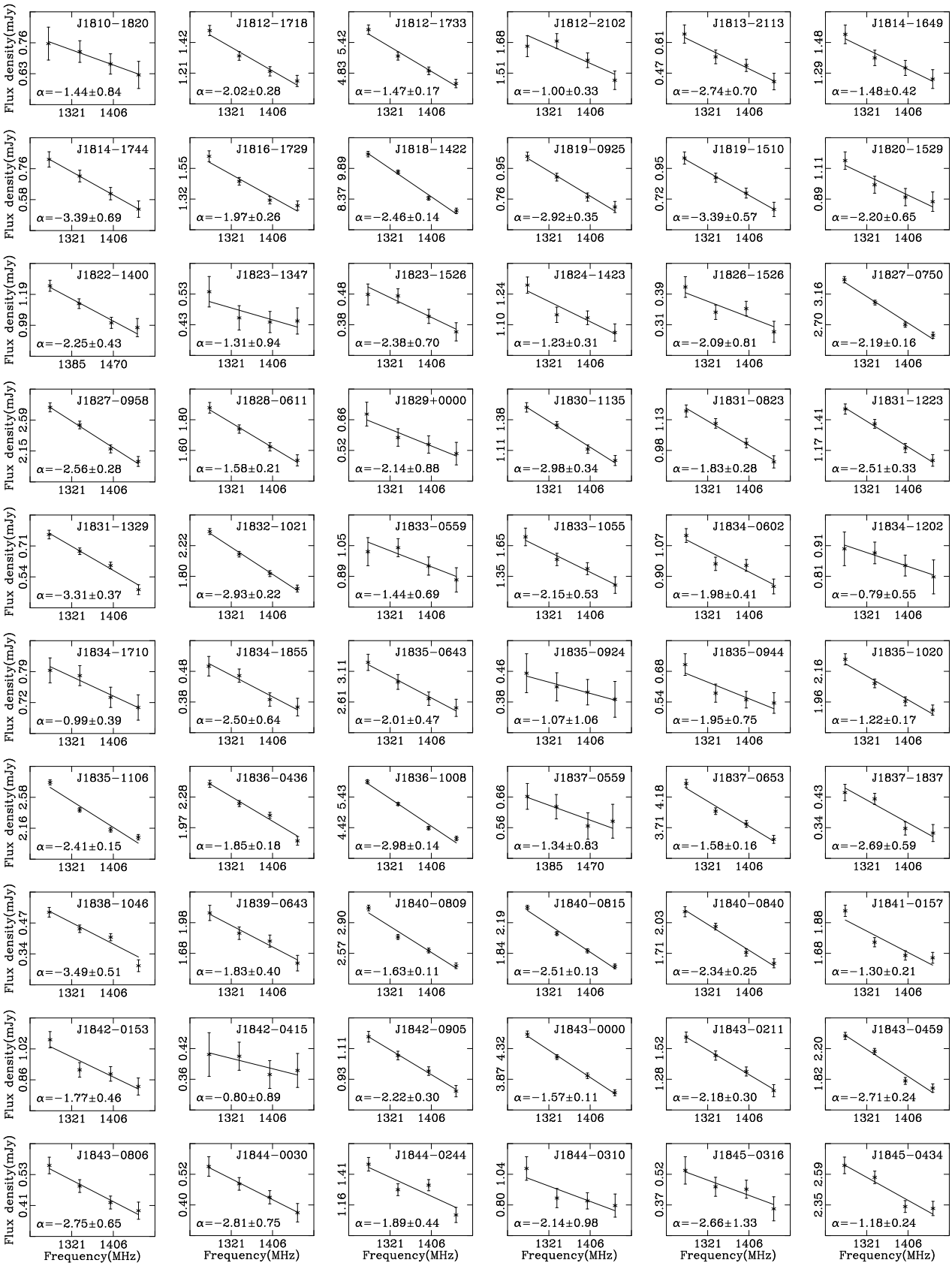

Fig. 2 — *Continued.*

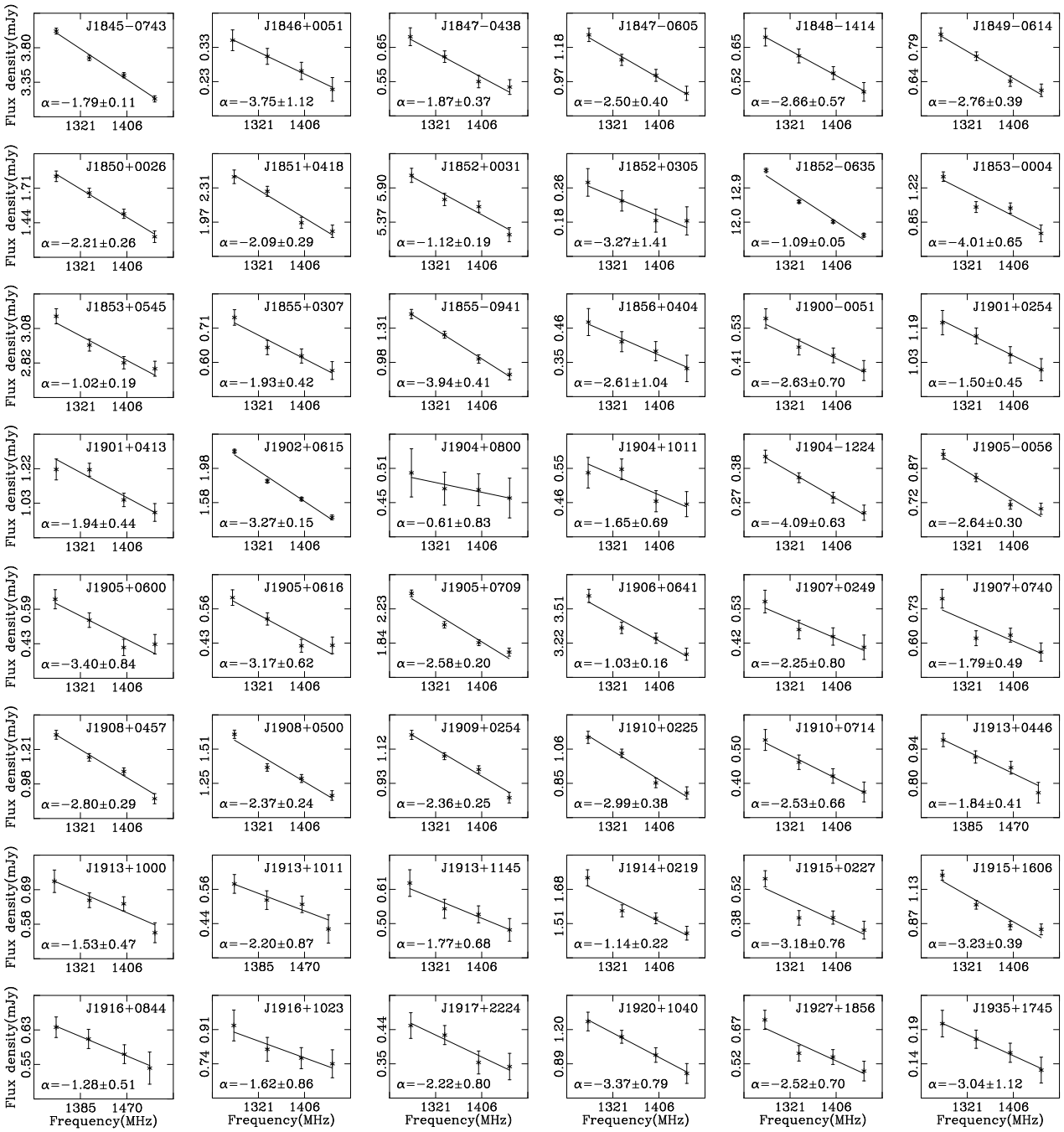

Fig. 2 — *Continued.*

pulsar rotation period P, the spin-down rate $\dot{P}$, the characteristic age $\tau = P/2\dot{P}$, the surface magnetic field strength $B_{\rm S} \propto \sqrt{P\dot{P}}$, the spin-down energy loss rate $\dot{E} \propto \dot{P}/P^3$, and also the potential drop in the polar gap $\Delta\Psi \propto P^{-3/2}\dot{P}^{1/2}$ which is related to particle acceleration. The Spearman rank correlation parameter (r) is used to describe the degree of correlation (Press et al. 1992), in which $r = 1$ stands for strong correlation and $r = 0$ for no correlation. We confirm the conclusion of previous authors (e.g. Lorimer et al. 1995) that there are some very weak correlations ($r \sim 0.3$) between spectral indices and $\dot{E}$ and $\Delta\Psi$ (see Table 4), which implies that the emission properties are physically related to the particle acceleration process.

4 CONCLUSIONS

We obtained the flux densities in four subbands for 228 pulsars observed by the Parkes 64 m telescope at 1.4 GHz, and determined their spectral indices, among which 200 are obtained for the first time. The indices have a broad

Table 2 The flux densities (S_i, in mJy) at four subbands (frequency in MHz) and spectral indices α that we obtained for 228 pulsars. Their DMs (in cm^{-3} pc) are listed after the pulsar names.

Pulsar Name	DM	Frequency1 / S_1	Frequency2 / S_2	Frequency3 / S_3	Frequency4 / S_4	α
J0719–2545	253.89	1278.75 / 1.00±0.02	1336.75 / 0.87±0.02	1400.29 / 0.82±0.02	1459.32 / 0.76±0.02	-1.99 ± 0.25
J0738–4042	160.80	1277.35 / 103.86±0.15	1337.61 / 91.67±0.10	1400.04 / 83.71±0.08	1460.04 / 80.83±0.11	-1.89 ± 0.01
J0818–3232	131.80	1278.75 / 1.07±0.02	1336.75 / 0.95±0.02	1400.29 / 0.86±0.02	1459.32 / 0.77±0.02	-2.41 ± 0.20
J0820–3921	179.40	1277.06 / 0.69±0.05	1337.61 / 0.58±0.03	1400.04 / 0.56±0.03	1460.04 / 0.50±0.03	-2.08 ± 0.58
J0821–4221	270.60	1276.68 / 0.70±0.03	1337.61 / 0.58±0.02	1400.04 / 0.51±0.02	1460.04 / 0.46±0.02	-3.15 ± 0.49
J0831–4406	254.00	1276.05 / 0.70±0.04	1337.61 / 0.64±0.02	1400.04 / 0.59±0.02	1461.16 / 0.60±0.03	-1.10 ± 0.47
J0838–2621	116.90	1277.10 / 0.65±0.04	1337.79 / 0.46±0.03	1400.04 / 0.40±0.02	1460.04 / 0.34±0.03	-4.84 ± 0.74
J0843–5022	178.47	1277.14 / 0.51±0.03	1337.36 / 0.46±0.02	1400.04 / 0.41±0.02	1460.04 / 0.39±0.02	-1.99 ± 0.61
J0932–3217	102.10	1277.64 / 0.45±0.02	1337.09 / 0.40±0.01	1400.60 / 0.32±0.01	1459.61 / 0.33±0.01	-2.74 ± 0.43
J0942–5552	180.20	1277.30 / 12.38±0.07	1336.75 / 10.65±0.05	1400.45 / 9.57±0.04	1459.61 / 8.64±0.05	-2.64 ± 0.05
J0945–4833	101.10	1278.75 / 0.47±0.02	1336.75 / 0.38±0.02	1400.29 / 0.35±0.02	1459.32 / 0.33±0.02	-2.73 ± 0.53
J0952–3839	167.00	1277.15 / 0.54±0.03	1337.61 / 0.40±0.02	1400.20 / 0.34±0.02	1460.04 / 0.31±0.02	-4.27 ± 0.54
J1017–5621	438.70	1278.75 / 2.56±0.03	1336.26 / 2.23±0.02	1400.29 / 2.01±0.02	1459.32 / 1.82±0.02	-2.56 ± 0.11
J1032–5911	418.20	1277.39 / 1.16±0.04	1337.61 / 0.93±0.03	1400.04 / 0.79±0.02	1460.04 / 0.77±0.03	-3.24 ± 0.37
J1058–5957	334.00	1277.39 / 0.75±0.02	1337.61 / 0.67±0.02	1400.04 / 0.60±0.02	1460.04 / 0.53±0.02	-2.57 ± 0.33
J1107–5947	158.40	1278.17 / 1.01±0.04	1336.91 / 1.00±0.03	1400.04 / 0.87±0.02	1460.04 / 0.85±0.03	-1.59 ± 0.36
J1107–6143	406.00	1342.75 / 0.74±0.01	1399.99 / 0.71±0.01	1465.60 / 0.65±0.01	1522.10 / 0.60±0.02	-1.58 ± 0.23
J1115–6052	228.20	1342.75 / 0.52±0.03	1399.88 / 0.46±0.02	1465.27 / 0.48±0.02	1521.94 / 0.44±0.03	-1.06 ± 0.61
J1123–6651	111.20	1277.30 / 0.53±0.06	1336.75 / 0.46±0.04	1400.60 / 0.42±0.03	1459.61 / 0.39±0.05	-2.34 ± 1.08
J1130–6807	148.73	1277.10 / 0.80±0.07	1336.91 / 0.64±0.05	1400.20 / 0.55±0.05	1460.04 / 0.49±0.06	-3.62 ± 0.96
J1156–5707	243.50	1276.14 / 0.39±0.04	1337.61 / 0.35±0.02	1400.20 / 0.31±0.02	1460.04 / 0.29±0.03	-2.24 ± 0.86
J1220–6318	347.00	1277.39 / 1.03±0.03	1337.44 / 0.93±0.02	1400.29 / 0.78±0.02	1459.52 / 0.72±0.03	-2.87 ± 0.33
J1225–6035	176.10	1278.75 / 0.36±0.02	1337.08 / 0.34±0.02	1400.29 / 0.31±0.02	1459.32 / 0.29±0.02	-1.69 ± 0.62
J1237–6725	176.50	1277.19 / 1.02±0.03	1336.75 / 0.75±0.02	1400.29 / 0.68±0.01	1459.32 / 0.53±0.02	-4.48 ± 0.27
J1303–6305	343.00	1277.16 / 0.38±0.03	1336.75 / 0.29±0.02	1400.29 / 0.28±0.02	1459.32 / 0.23±0.02	-3.36 ± 0.85
J1314–6101	309.00	1277.10 / 0.78±0.03	1336.91 / 0.64±0.02	1400.04 / 0.57±0.02	1460.04 / 0.51±0.02	-3.09 ± 0.40
J1319–6105	442.20	1278.50 / 1.48±0.04	1336.75 / 1.38±0.03	1400.45 / 1.28±0.03	1459.32 / 1.26±0.03	-1.27 ± 0.24
J1326–6408	502.70	1278.75 / 2.85±0.03	1336.75 / 2.40±0.02	1400.29 / 2.16±0.02	1459.32 / 2.00±0.03	-2.71 ± 0.12
J1348–6307	597.00	1277.70 / 0.71±0.04	1337.09 / 0.60±0.02	1400.45 / 0.49±0.02	1459.61 / 0.49±0.03	-3.06 ± 0.53
J1352–6803	214.60	1278.75 / 1.90±0.04	1336.75 / 1.66±0.03	1400.29 / 1.42±0.03	1459.52 / 1.30±0.03	-2.99 ± 0.22
J1355–5925	354.80	1342.75 / 0.75±0.02	1399.59 / 0.70±0.02	1465.35 / 0.64±0.02	1522.34 / 0.63±0.03	-1.52 ± 0.36
J1412–6111	311.80	1275.57 / 0.62±0.05	1337.61 / 0.57±0.03	1400.04 / 0.50±0.03	1460.04 / 0.46±0.03	-2.27 ± 0.67
J1415–6621	260.17	1278.75 / 0.59±0.03	1336.91 / 0.51±0.02	1400.29 / 0.45±0.02	1459.32 / 0.45±0.02	-2.13 ± 0.47
J1424–5556	198.70	1277.64 / 0.55±0.03	1336.75 / 0.51±0.02	1400.60 / 0.45±0.02	1459.11 / 0.45±0.03	-1.65 ± 0.56
J1444–5941	177.10	1277.49 / 0.83±0.05	1336.75 / 0.68±0.03	1400.29 / 0.62±0.03	1459.61 / 0.56±0.03	-2.85 ± 0.58
J1502–6128	256.50	1277.39 / 0.87±0.03	1337.61 / 0.69±0.02	1400.04 / 0.61±0.02	1460.04 / 0.60±0.03	-2.95 ± 0.41
J1507–6640	129.80	1277.10 / 1.41±0.02	1336.91 / 1.23±0.02	1400.20 / 1.05±0.02	1460.04 / 0.97±0.02	-2.96 ± 0.17
J1511–5835	332.00	1277.18 / 0.91±0.05	1336.91 / 0.81±0.03	1399.87 / 0.74±0.03	1460.04 / 0.57±0.03	-3.09 ± 0.56
J1524–5706	833.00	1342.50 / 0.47±0.02	1399.88 / 0.41±0.02	1465.39 / 0.40±0.02	1523.09 / 0.38±0.02	-1.56 ± 0.49
J1534–5405	190.82	1278.50 / 1.99±0.04	1336.75 / 1.63±0.03	1400.29 / 1.39±0.03	1459.11 / 1.26±0.04	-3.55 ± 0.24
J1537–5645	707.00	1277.28 / 1.41±0.08	1337.61 / 1.31±0.06	1400.04 / 1.26±0.05	1460.04 / 1.22±0.06	-1.04 ± 0.51
J1548–4927	141.20	1278.75 / 0.75±0.03	1336.75 / 0.66±0.02	1400.44 / 0.62±0.02	1459.32 / 0.52±0.02	-2.48 ± 0.37
J1553–5456	210.00	1278.75 / 1.36±0.04	1336.75 / 1.16±0.03	1400.29 / 0.93±0.03	1459.32 / 0.87±0.03	-3.60 ± 0.29
J1614–3937	152.44	1277.28 / 0.55±0.04	1336.91 / 0.51±0.03	1400.20 / 0.42±0.02	1460.04 / 0.43±0.03	-2.05 ± 0.66
J1615–5537	124.48	1277.11 / 1.11±0.03	1336.91 / 0.98±0.02	1400.20 / 0.91±0.02	1460.04 / 0.82±0.03	-2.14 ± 0.30
J1622–4802	364.30	1277.28 / 0.91±0.04	1337.61 / 0.86±0.02	1400.04 / 0.82±0.02	1460.04 / 0.82±0.03	-0.84 ± 0.36
J1623–4256	295.00	1277.38 / 2.93±0.08	1336.91 / 2.64±0.06	1400.20 / 2.40±0.05	1460.04 / 2.41±0.07	-1.57 ± 0.27
J1624–4411	139.40	1277.17 / 0.57±0.04	1336.91 / 0.50±0.03	1400.20 / 0.48±0.03	1460.04 / 0.46±0.03	-1.39 ± 0.65
J1626–4537	237.00	1277.45 / 1.08±0.03	1337.09 / 0.98±0.02	1400.60 / 0.91±0.02	1459.61 / 0.89±0.02	-1.49 ± 0.26
J1627–4845	557.80	1277.56 / 0.68±0.07	1336.75 / 0.63±0.04	1400.44 / 0.61±0.04	1459.61 / 0.59±0.05	-0.92 ± 0.87
J1627–5547	166.20	1342.75 / 0.67±0.02	1399.76 / 0.58±0.02	1465.60 / 0.56±0.02	1522.34 / 0.50±0.03	-2.15 ± 0.43
J1628–4804	952.00	1274.90 / 1.38±0.08	1337.07 / 1.29±0.06	1399.87 / 1.12±0.05	1460.04 / 1.13±0.06	-1.68 ± 0.55
J1632–4621	562.90	1278.75 / 1.08±0.03	1336.75 / 0.95±0.02	1400.12 / 0.84±0.02	1459.96 / 0.78±0.03	-2.52 ± 0.31

distribution in the range from -4.8 to -0.5. Such observations for getting spectral indices have a few advantages: (1) flux densities are measured by a single instrument and calibrated with a consistent approach using the same flux calibrator; (2) one observation session can avoid the short-term scintillation effect when the DM is large enough and also avoids long-term flux changes due to diffractive and reflective scintillation; (3) in such a small frequency range

Table 2 — *Continued.*

Pulsar Name	DM	Frequency1 / S_1	Frequency2 / S_2	Frequency3 / S_3	Frequency4 / S_4	α
J1635–5954	134.90	1277.31 / 2.15±0.04	1336.91 / 1.84±0.02	1400.20 / 1.56±0.02	1460.04 / 1.39±0.03	-3.35 ± 0.17
J1636–4803	503.00	1278.75 / 2.27±0.08	1336.75 / 1.95±0.06	1400.12 / 1.80±0.06	1459.32 / 1.67±0.06	-2.26 ± 0.36
J1636–4933	542.70	1277.31 / 0.69±0.06	1336.91 / 0.67±0.04	1400.03 / 0.47±0.03	1460.04 / 0.44±0.04	-4.28 ± 0.80
J1637–4721	448.00	1277.19 / 0.87±0.06	1336.91 / 0.76±0.04	1400.03 / 0.72±0.04	1460.04 / 0.61±0.04	-2.41 ± 0.70
J1638–3815	238.00	1277.32 / 0.85±0.04	1337.13 / 0.70±0.02	1400.20 / 0.67±0.02	1460.04 / 0.61±0.03	-2.26 ± 0.44
J1638–5226	170.10	1277.39 / 0.75±0.03	1337.61 / 0.66±0.02	1400.20 / 0.59±0.02	1460.04 / 0.56±0.03	-2.29 ± 0.45
J1644–4559	478.80	1276.39 / 405.85±0.22	1337.07 / 342.68±0.13	1399.87 / 296.43±0.10	1460.04 / 272.71±0.10	-2.90 ± 0.00
J1648–4458	925.00	1276.91 / 0.64±0.08	1337.61 / 0.57±0.05	1399.87 / 0.54±0.04	1460.04 / 0.47±0.05	-2.17 ± 1.14
J1649–3805	213.80	1277.14 / 1.54±0.05	1337.61 / 1.23±0.03	1400.20 / 1.16±0.03	1460.04 / 1.15±0.04	-2.12 ± 0.30
J1649–4653	332.00	1277.32 / 0.38±0.05	1336.91 / 0.36±0.03	1400.03 / 0.34±0.03	1460.04 / 0.28±0.03	-2.17 ± 1.18
J1651–4246	482.00	1277.69 / 23.34±0.17	1336.75 / 21.23±0.12	1400.29 / 18.61±0.10	1459.61 / 16.99±0.12	-2.46 ± 0.07
J1651–5255	164.00	1277.04 / 3.96±0.05	1336.75 / 3.41±0.03	1400.60 / 2.89±0.03	1459.61 / 2.65±0.04	-3.11 ± 0.13
J1658–4958	193.40	1278.75 / 2.11±0.04	1336.75 / 1.89±0.03	1400.44 / 1.63±0.03	1459.32 / 1.53±0.04	-2.56 ± 0.21
J1659–4439	535.00	1277.25 / 0.50±0.04	1336.91 / 0.44±0.03	1400.03 / 0.44±0.02	1460.04 / 0.42±0.03	-1.10 ± 0.74
J1700–3611	232.70	1277.13 / 1.11±0.05	1337.07 / 0.99±0.03	1400.20 / 0.92±0.03	1460.04 / 0.79±0.03	-2.27 ± 0.41
J1702–4217	629.00	1276.88 / 1.36±0.16	1337.07 / 1.30±0.10	1399.87 / 1.18±0.08	1460.26 / 1.18±0.10	-1.23 ± 0.93
J1705–3950	207.10	1278.75 / 2.01±0.06	1336.75 / 1.92±0.05	1400.12 / 1.77±0.05	1459.32 / 1.83±0.05	-0.84 ± 0.30
J1707–4053	360.00	1277.26 / 12.24±0.24	1336.91 / 10.21±0.17	1400.15 / 8.84±0.15	1460.04 / 8.31±0.18	-2.99 ± 0.20
J1707–4341	398.20	1342.75 / 0.60±0.03	1399.86 / 0.53±0.02	1465.60 / 0.48±0.02	1522.10 / 0.49±0.03	-1.85 ± 0.50
J1707–4729	268.30	1278.75 / 2.87±0.10	1336.75 / 2.71±0.08	1400.44 / 2.66±0.08	1459.32 / 2.46±0.09	-1.04 ± 0.35
J1708–3827	788.00	1276.78 / 0.52±0.05	1336.75 / 0.54±0.03	1400.29 / 0.44±0.03	1459.61 / 0.40±0.03	-2.53 ± 0.85
J1709–3626	393.60	1276.22 / 0.63±0.05	1337.07 / 0.61±0.03	1400.04 / 0.57±0.03	1460.04 / 0.57±0.04	-0.84 ± 0.68
J1715–4034	254.00	1278.75 / 2.40±0.04	1337.08 / 2.07±0.03	1400.12 / 1.86±0.03	1459.52 / 1.74±0.03	-2.48 ± 0.17
J1716–3720	682.70	1276.91 / 0.57±0.04	1336.91 / 0.49±0.02	1400.03 / 0.38±0.02	1460.04 / 0.37±0.03	-3.75 ± 0.68
J1717–3953	466.00	1277.70 / 1.77±0.07	1337.09 / 1.58±0.06	1400.29 / 1.28±0.05	1459.61 / 1.17±0.06	-3.33 ± 0.45
J1718–3718	371.10	1276.72 / 3.03±0.26	1336.89 / 2.55±0.18	1399.87 / 2.16±0.17	1460.21 / 1.84±0.18	-3.69 ± 0.89
J1719–4302	297.70	1276.31 / 0.51±0.04	1336.75 / 0.45±0.03	1400.44 / 0.40±0.02	1459.32 / 0.31±0.03	-3.33 ± 0.85
J1724–3149	409.00	1278.09 / 0.49±0.05	1336.91 / 0.44±0.03	1400.20 / 0.43±0.03	1460.04 / 0.39±0.03	-1.49 ± 0.88
J1725–3546	744.00	1276.62 / 1.01±0.06	1337.07 / 0.93±0.04	1399.87 / 0.71±0.03	1460.04 / 0.61±0.04	-4.07 ± 0.61
J1727–2739	147.00	1278.75 / 4.04±0.05	1336.75 / 3.59±0.04	1400.44 / 3.28±0.04	1459.52 / 3.09±0.05	-2.04 ± 0.14
J1728–4028	231.00	1277.69 / 1.12±0.05	1336.75 / 1.02±0.03	1400.60 / 0.90±0.03	1460.07 / 0.77±0.04	-2.82 ± 0.42
J1730–3353	256.00	1278.02 / 0.51±0.04	1336.91 / 0.46±0.03	1400.03 / 0.39±0.03	1460.04 / 0.28±0.03	-4.08 ± 0.90
J1732–4128	195.30	1276.57 / 1.37±0.04	1337.61 / 1.09±0.02	1400.44 / 1.01±0.02	1459.52 / 0.93±0.03	-2.76 ± 0.27
J1733–3322	524.00	1342.75 / 1.23±0.04	1399.98 / 1.14±0.03	1465.75 / 0.98±0.03	1521.58 / 0.83±0.04	-2.96 ± 0.38
J1733–4005	317.80	1276.84 / 0.81±0.03	1336.91 / 0.68±0.02	1400.20 / 0.57±0.02	1460.04 / 0.53±0.02	-3.32 ± 0.34
J1736–2457	170.00	1276.90 / 1.17±0.04	1336.91 / 0.99±0.02	1400.20 / 0.84±0.02	1460.04 / 0.76±0.02	-3.24 ± 0.30
J1736–2843	331.00	1277.32 / 0.49±0.03	1336.91 / 0.43±0.02	1400.20 / 0.36±0.02	1460.78 / 0.32±0.02	-3.16 ± 0.68
J1737–3102	280.00	1275.83 / 0.77±0.04	1337.32 / 0.65±0.03	1399.70 / 0.57±0.02	1460.04 / 0.57±0.03	-2.26 ± 0.49
J1737–3137	488.20	1278.50 / 1.20±0.07	1336.75 / 1.06±0.06	1400.12 / 0.98±0.05	1459.11 / 1.01±0.06	-1.33 ± 0.58
J1738–2330	99.30	1277.32 / 1.47±0.06	1336.91 / 1.21±0.04	1400.20 / 1.05±0.03	1460.04 / 0.88±0.05	-3.69 ± 0.42
J1738–2647	182.20	1277.25 / 0.70±0.04	1336.91 / 0.53±0.03	1400.20 / 0.50±0.02	1460.04 / 0.48±0.03	-2.74 ± 0.58
J1738–3316	273.00	1275.67 / 0.92±0.07	1337.07 / 0.69±0.04	1400.04 / 0.62±0.04	1460.04 / 0.53±0.05	-3.83 ± 0.77
J1739–3159	337.00	1277.70 / 1.10±0.07	1337.09 / 1.06±0.04	1400.29 / 0.98±0.04	1459.61 / 0.81±0.05	-2.21 ± 0.58
J1740–3052	738.78	1278.75 / 1.14±0.05	1336.75 / 0.90±0.04	1399.95 / 0.79±0.04	1459.32 / 0.74±0.04	-3.39 ± 0.54
J1741–2733	149.20	1278.50 / 3.02±0.06	1336.75 / 2.67±0.05	1400.45 / 2.34±0.04	1459.32 / 2.18±0.05	-2.52 ± 0.21
J1741–3016	382.00	1278.75 / 3.49±0.08	1336.75 / 3.06±0.05	1399.95 / 2.74±0.05	1459.32 / 2.71±0.06	-1.98 ± 0.21
J1744–3130	192.90	1276.42 / 0.81±0.04	1337.61 / 0.66±0.02	1400.04 / 0.67±0.02	1460.29 / 0.61±0.03	-1.66 ± 0.41
J1749–2629	409.00	1342.50 / 0.74±0.04	1399.99 / 0.72±0.03	1465.39 / 0.62±0.03	1522.35 / 0.55±0.04	-2.38 ± 0.59
J1750–2438	476.00	1275.87 / 0.83±0.03	1337.07 / 0.63±0.02	1400.04 / 0.55±0.02	1460.04 / 0.49±0.02	-3.82 ± 0.38
J1751–3323	296.70	1278.50 / 2.19±0.05	1336.92 / 1.95±0.04	1400.60 / 1.91±0.04	1459.52 / 1.74±0.05	-1.53 ± 0.24
J1754–3443	187.70	1276.70 / 0.77±0.04	1336.91 / 0.63±0.02	1400.20 / 0.61±0.02	1460.04 / 0.58±0.02	-1.82 ± 0.43
J1755–2725	115.00	1277.56 / 1.16±0.11	1336.75 / 1.01±0.07	1400.60 / 0.94±0.06	1459.61 / 0.91±0.07	-1.74 ± 0.84
J1756–2251	121.20	1276.34 / 0.94±0.05	1336.75 / 0.94±0.03	1400.60 / 0.81±0.03	1459.61 / 0.80±0.03	-1.67 ± 0.43
J1757–2223	239.30	1278.75 / 1.36±0.07	1336.91 / 1.32±0.05	1400.29 / 1.35±0.05	1459.52 / 1.25±0.05	-0.46 ± 0.44
J1758–2206	678.00	1276.46 / 0.63±0.06	1336.91 / 0.54±0.04	1400.20 / 0.43±0.03	1460.04 / 0.42±0.04	-3.36 ± 0.95
J1758–2540	218.20	1276.69 / 1.06±0.06	1336.91 / 0.86±0.04	1399.89 / 0.72±0.03	1460.04 / 0.75±0.04	-2.73 ± 0.55
J1758–2630	328.00	1276.17 / 0.23±0.03	1336.91 / 0.24±0.02	1400.20 / 0.22±0.02	1460.04 / 0.20±0.02	-1.28 ± 1.09
J1759–1940	302.70	1276.34 / 1.49±0.09	1337.07 / 1.32±0.06	1400.04 / 1.11±0.05	1460.26 / 1.10±0.07	-2.54 ± 0.57
J1759–3107	128.60	1342.75 / 1.66±0.03	1400.15 / 1.52±0.02	1465.39 / 1.43±0.02	1521.98 / 1.31±0.03	-1.82 ± 0.18
J1801–1909	264.00	1277.08 / 0.77±0.04	1336.91 / 0.63±0.02	1400.20 / 0.51±0.02	1460.04 / 0.45±0.03	-4.23 ± 0.53

Table 2 — *Continued.*

Pulsar Name	DM	Frequency1 / S_1	Frequency2 / S_2	Frequency3 / S_3	Frequency4 / S_4	α
J1802–2124	149.63	1342.50 / 1.01±0.03	1400.15 / 0.89±0.03	1465.15 / 0.75±0.03	1521.66 / 0.63±0.03	-3.73 ± 0.44
J1802–2426	711.00	1276.92 / 0.48±0.04	1337.07 / 0.46±0.03	1399.89 / 0.42±0.03	1460.04 / 0.39±0.03	-1.60 ± 0.80
J1803–1857	392.00	1277.96 / 0.45±0.02	1336.91 / 0.39±0.01	1400.20 / 0.37±0.01	1460.04 / 0.36±0.02	-1.59 ± 0.46
J1804–0735	186.32	1277.01 / 1.02±0.07	1336.75 / 0.99±0.05	1400.76 / 0.84±0.05	1459.83 / 0.77±0.05	-2.35 ± 0.67
J1805–1504	225.00	1277.10 / 5.40±0.09	1337.07 / 4.79±0.05	1400.04 / 4.32±0.05	1460.78 / 4.23±0.06	-1.83 ± 0.14
J1806–1154	122.41	1278.75 / 3.48±0.04	1336.75 / 3.00±0.03	1400.29 / 2.50±0.03	1459.52 / 2.36±0.03	-3.14 ± 0.13
J1809–1429	411.30	1278.75 / 1.07±0.04	1336.75 / 0.91±0.03	1400.29 / 0.83±0.03	1459.32 / 0.80±0.03	-2.19 ± 0.35
J1810–1820	452.20	1275.64 / 0.76±0.07	1337.07 / 0.72±0.05	1399.89 / 0.67±0.04	1460.26 / 0.63±0.05	-1.44 ± 0.84
J1812–1718	255.10	1278.50 / 1.52±0.04	1336.75 / 1.33±0.03	1400.45 / 1.22±0.03	1459.11 / 1.16±0.03	-2.02 ± 0.28
J1812–1733	518.00	1278.50 / 5.68±0.10	1336.75 / 5.15±0.08	1400.45 / 4.87±0.07	1459.11 / 4.64±0.07	-1.47 ± 0.17
J1812–2102	547.20	1278.50 / 1.66±0.06	1336.75 / 1.69±0.04	1400.45 / 1.58±0.04	1459.11 / 1.48±0.05	-1.00 ± 0.33
J1813–2113	462.30	1275.34 / 0.65±0.05	1336.91 / 0.54±0.03	1400.20 / 0.50±0.03	1460.04 / 0.43±0.03	-2.74 ± 0.70
J1814–1649	782.00	1278.75 / 1.54±0.07	1337.08 / 1.38±0.05	1400.29 / 1.32±0.05	1459.32 / 1.25±0.05	-1.48 ± 0.42
J1814–1744	792.00	1276.87 / 0.83±0.06	1336.91 / 0.71±0.04	1400.04 / 0.61±0.03	1460.04 / 0.53±0.04	-3.39 ± 0.69
J1816–1729	525.50	1277.38 / 1.66±0.05	1336.91 / 1.45±0.03	1400.20 / 1.31±0.03	1460.04 / 1.27±0.03	-1.97 ± 0.26
J1818–1422	622.00	1277.75 / 10.69±0.16	1336.91 / 9.69±0.10	1400.04 / 8.41±0.09	1460.04 / 7.85±0.12	-2.46 ± 0.14
J1819–0925	378.00	1278.75 / 1.04±0.03	1336.75 / 0.89±0.03	1400.29 / 0.77±0.02	1459.52 / 0.72±0.03	-2.92 ± 0.35
J1819–1510	421.70	1275.39 / 1.04±0.06	1337.07 / 0.87±0.04	1399.89 / 0.76±0.03	1460.04 / 0.65±0.04	-3.39 ± 0.57
J1820–1529	772.00	1278.50 / 1.17±0.07	1336.75 / 0.99±0.06	1400.45 / 0.91±0.05	1459.32 / 0.88±0.06	-2.20 ± 0.65
J1822–1400	651.10	1342.75 / 1.26±0.04	1399.82 / 1.13±0.03	1466.05 / 1.00±0.03	1521.60 / 0.98±0.05	-2.25 ± 0.43
J1823–1347	1044.00	1277.56 / 0.54±0.06	1336.75 / 0.45±0.04	1400.45 / 0.44±0.03	1459.61 / 0.44±0.04	-1.31 ± 0.94
J1823–1526	611.00	1277.44 / 0.48±0.04	1336.75 / 0.47±0.03	1400.45 / 0.41±0.02	1459.61 / 0.36±0.02	-2.38 ± 0.70
J1824–1423	428.30	1278.75 / 1.28±0.04	1336.75 / 1.15±0.03	1400.29 / 1.13±0.03	1459.32 / 1.07±0.04	-1.23 ± 0.31
J1826–1526	530.00	1277.09 / 0.42±0.04	1336.91 / 0.34±0.02	1400.04 / 0.35±0.02	1460.04 / 0.29±0.02	-2.09 ± 0.81
J1827–0750	381.00	1277.14 / 3.41±0.06	1337.61 / 3.03±0.04	1400.04 / 2.70±0.04	1460.04 / 2.56±0.04	-2.19 ± 0.16
J1827–0958	430.00	1278.75 / 2.79±0.07	1336.91 / 2.51±0.06	1400.29 / 2.17±0.05	1459.32 / 2.02±0.06	-2.56 ± 0.28
J1828–0611	363.20	1278.50 / 1.89±0.04	1336.92 / 1.74±0.03	1400.45 / 1.62±0.03	1459.55 / 1.53±0.03	-1.58 ± 0.21
J1829+0000	114.00	1275.18 / 0.69±0.07	1336.91 / 0.57±0.04	1400.20 / 0.54±0.04	1460.04 / 0.50±0.05	-2.14 ± 0.88
J1830–1135	257.00	1277.18 / 1.51±0.05	1336.91 / 1.33±0.03	1400.80 / 1.12±0.03	1460.04 / 1.03±0.04	-2.98 ± 0.34
J1831–0823	245.90	1278.75 / 1.18±0.03	1336.91 / 1.11±0.02	1400.29 / 1.01±0.02	1459.75 / 0.93±0.03	-1.83 ± 0.28
J1831–1223	342.00	1278.75 / 1.50±0.05	1336.91 / 1.37±0.04	1400.29 / 1.18±0.03	1459.32 / 1.10±0.04	-2.51 ± 0.33
J1831–1329	338.00	1276.91 / 0.78±0.03	1336.91 / 0.67±0.02	1400.20 / 0.60±0.02	1460.04 / 0.49±0.02	-3.31 ± 0.37
J1832–1021	475.70	1278.75 / 2.44±0.05	1336.75 / 2.09±0.04	1400.29 / 1.83±0.04	1459.52 / 1.66±0.04	-2.93 ± 0.22
J1833–0559	353.00	1277.39 / 1.02±0.08	1337.07 / 1.04±0.05	1400.04 / 0.94±0.05	1460.04 / 0.87±0.06	-1.44 ± 0.69
J1833–1055	543.00	1275.09 / 1.75±0.10	1337.07 / 1.51±0.06	1400.04 / 1.42±0.06	1460.04 / 1.27±0.07	-2.15 ± 0.53
J1834–0602	445.00	1278.75 / 1.14±0.05	1336.75 / 0.97±0.04	1400.29 / 0.96±0.03	1459.32 / 0.85±0.04	-1.98 ± 0.41
J1834–1202	342.40	1277.15 / 0.90±0.05	1337.07 / 0.88±0.03	1400.04 / 0.84±0.03	1461.24 / 0.81±0.05	-0.79 ± 0.55
J1834–1710	123.80	1278.75 / 0.80±0.03	1337.08 / 0.78±0.02	1400.29 / 0.73±0.02	1459.32 / 0.71±0.03	-0.99 ± 0.39
J1834–1855	185.20	1276.86 / 0.49±0.03	1336.91 / 0.46±0.02	1400.20 / 0.39±0.02	1460.04 / 0.37±0.02	-2.50 ± 0.64
J1835–0643	472.90	1277.82 / 3.27±0.15	1336.75 / 2.92±0.12	1400.45 / 2.66±0.10	1459.61 / 2.52±0.12	-2.01 ± 0.47
J1835–0924	471.00	1277.07 / 0.46±0.05	1336.75 / 0.42±0.04	1400.45 / 0.41±0.03	1459.54 / 0.39±0.04	-1.07 ± 1.06
J1835–0944	277.20	1276.74 / 0.72±0.06	1336.91 / 0.58±0.04	1400.04 / 0.55±0.03	1460.04 / 0.54±0.04	-1.95 ± 0.75
J1835–1020	113.70	1278.75 / 2.24±0.04	1336.91 / 2.08±0.03	1400.29 / 1.96±0.03	1459.32 / 1.91±0.03	-1.22 ± 0.17
J1835–1106	132.68	1278.75 / 2.81±0.04	1336.75 / 2.40±0.03	1400.29 / 2.14±0.03	1459.52 / 2.05±0.03	-2.41 ± 0.15
J1836–0436	231.50	1278.75 / 2.43±0.04	1337.08 / 2.21±0.03	1400.29 / 2.09±0.03	1459.96 / 1.86±0.04	-1.85 ± 0.18
J1836–1008	316.98	1276.45 / 6.02±0.08	1337.07 / 5.18±0.05	1400.04 / 4.40±0.05	1460.26 / 4.11±0.06	-2.98 ± 0.14
J1837–0559	317.80	1342.75 / 0.67±0.05	1400.12 / 0.63±0.04	1465.36 / 0.57±0.04	1518.87 / 0.58±0.05	-1.34 ± 0.83
J1837–0653	316.10	1278.75 / 4.41±0.07	1336.91 / 3.96±0.05	1400.29 / 3.76±0.05	1459.52 / 3.54±0.06	-1.58 ± 0.16
J1837–1837	100.74	1278.21 / 0.44±0.03	1336.91 / 0.42±0.02	1400.20 / 0.34±0.02	1460.04 / 0.33±0.02	-2.69 ± 0.59
J1838–1046	208.00	1277.18 / 0.53±0.03	1336.91 / 0.44±0.02	1400.41 / 0.41±0.01	1460.04 / 0.31±0.02	-3.49 ± 0.51
J1839–0643	497.90	1278.75 / 2.08±0.08	1336.91 / 1.87±0.06	1400.29 / 1.79±0.06	1459.96 / 1.59±0.07	-1.83 ± 0.40
J1840–0809	349.80	1278.75 / 3.07±0.03	1336.75 / 2.74±0.03	1400.29 / 2.60±0.02	1459.52 / 2.45±0.03	-1.63 ± 0.11
J1840–0815	233.20	1278.75 / 2.39±0.03	1336.91 / 2.06±0.02	1400.29 / 1.87±0.02	1459.52 / 1.71±0.02	-2.51 ± 0.13
J1840–0840	272.00	1276.49 / 2.16±0.06	1336.91 / 1.99±0.04	1400.04 / 1.72±0.03	1460.04 / 1.61±0.04	-2.34 ± 0.25
J1841–0157	475.00	1278.75 / 1.97±0.04	1336.75 / 1.75±0.03	1400.29 / 1.66±0.03	1459.32 / 1.65±0.03	-1.30 ± 0.21
J1842–0153	434.00	1278.75 / 1.07±0.05	1336.75 / 0.91±0.04	1400.29 / 0.89±0.04	1459.52 / 0.83±0.04	-1.77 ± 0.46
J1842–0415	188.00	1277.49 / 0.40±0.04	1336.91 / 0.40±0.03	1400.04 / 0.37±0.02	1460.04 / 0.37±0.03	-0.80 ± 0.89
J1842–0905	343.30	1278.75 / 1.18±0.04	1336.75 / 1.06±0.03	1400.29 / 0.97±0.02	1459.32 / 0.87±0.03	-2.22 ± 0.30
J1843–0000	101.50	1278.75 / 4.55±0.05	1337.08 / 4.19±0.04	1400.29 / 3.92±0.04	1459.32 / 3.69±0.04	-1.57 ± 0.11
J1843–0211	441.70	1278.75 / 1.62±0.05	1336.91 / 1.46±0.04	1400.29 / 1.34±0.03	1459.52 / 1.20±0.04	-2.18 ± 0.30
J1843–0459	444.10	1278.75 / 2.38±0.05	1336.75 / 2.16±0.04	1400.29 / 1.80±0.04	1459.52 / 1.72±0.05	-2.71 ± 0.24

Table 2 — *Continued.*

Pulsar Name	DM	Frequency1 / S_1	Frequency2 / S_2	Frequency3 / S_3	Frequency4 / S_4	α
J1843–0806	215.80	1277.34 / 0.57±0.04	1336.91 / 0.48±0.02	1400.04 / 0.42±0.02	1460.04 / 0.39±0.03	-2.75 ± 0.65
J1844–0030	605.00	1276.90 / 0.55±0.05	1336.91 / 0.48±0.03	1400.04 / 0.43±0.02	1460.04 / 0.38±0.03	-2.81 ± 0.75
J1844–0244	429.00	1278.75 / 1.50±0.06	1336.75 / 1.28±0.05	1400.29 / 1.32±0.05	1459.32 / 1.09±0.05	-1.89 ± 0.44
J1844–0310	836.10	1277.11 / 1.09±0.11	1337.07 / 0.84±0.07	1400.04 / 0.82±0.06	1460.04 / 0.79±0.08	-2.14 ± 0.98
J1845–0316	500.00	1277.04 / 0.54±0.08	1336.75 / 0.45±0.05	1400.45 / 0.44±0.04	1459.61 / 0.35±0.05	-2.66 ± 1.33
J1845–0434	230.80	1277.39 / 2.67±0.07	1337.07 / 2.57±0.05	1400.04 / 2.34±0.04	1460.04 / 2.32±0.05	-1.18 ± 0.24
J1845–0743	281.00	1278.75 / 4.03±0.04	1336.75 / 3.66±0.04	1400.29 / 3.44±0.03	1459.52 / 3.15±0.04	-1.79 ± 0.11
J1846+0051	140.00	1275.45 / 0.36±0.04	1336.91 / 0.30±0.03	1400.04 / 0.26±0.02	1460.04 / 0.21±0.03	-3.75 ± 1.12
J1847–0438	229.00	1276.31 / 0.68±0.03	1337.07 / 0.62±0.02	1400.04 / 0.55±0.02	1460.26 / 0.54±0.02	-1.87 ± 0.37
J1847–0605	207.90	1278.75 / 1.27±0.05	1336.75 / 1.10±0.04	1400.29 / 1.01±0.04	1459.52 / 0.91±0.04	-2.50 ± 0.40
J1848–1414	134.47	1277.56 / 0.70±0.04	1336.75 / 0.61±0.03	1400.60 / 0.55±0.02	1459.61 / 0.48±0.03	-2.66 ± 0.57
J1849–0614	119.60	1274.49 / 0.86±0.04	1337.32 / 0.75±0.02	1400.04 / 0.64±0.02	1460.26 / 0.60±0.02	-2.76 ± 0.39
J1850+0026	201.40	1278.75 / 1.81±0.05	1336.75 / 1.67±0.04	1400.29 / 1.51±0.03	1459.32 / 1.35±0.04	-2.21 ± 0.26
J1851+0418	115.54	1278.20 / 2.43±0.08	1336.91 / 2.27±0.05	1400.03 / 1.96±0.05	1460.04 / 1.89±0.05	-2.09 ± 0.29
J1852+0031	787.00	1278.50 / 6.11±0.12	1336.92 / 5.72±0.10	1400.45 / 5.60±0.09	1459.32 / 5.18±0.10	-1.12 ± 0.19
J1852+0305	320.00	1276.95 / 0.27±0.04	1337.07 / 0.22±0.02	1400.04 / 0.18±0.02	1460.04 / 0.18±0.03	-3.27 ± 1.41
J1852–0635	171.00	1278.75 / 13.44±0.06	1337.08 / 12.52±0.05	1400.29 / 11.97±0.05	1459.52 / 11.6±0.05	-1.09 ± 0.05
J1853–0004	438.20	1278.75 / 1.37±0.07	1336.75 / 0.99±0.06	1400.29 / 0.98±0.05	1459.52 / 0.75±0.07	-4.01 ± 0.65
J1853+0545	198.70	1278.75 / 3.18±0.06	1337.08 / 2.95±0.05	1400.29 / 2.82±0.05	1459.96 / 2.78±0.05	-1.02 ± 0.19
J1855+0307	402.50	1278.75 / 0.75±0.03	1336.99 / 0.65±0.02	1400.29 / 0.62±0.02	1459.52 / 0.57±0.03	-1.93 ± 0.42
J1855–0941	151.99	1278.27 / 1.48±0.06	1336.91 / 1.24±0.04	1400.20 / 1.01±0.04	1460.04 / 0.89±0.04	-3.94 ± 0.41
J1856+0404	341.30	1278.01 / 0.49±0.05	1336.91 / 0.42±0.03	1399.87 / 0.38±0.03	1460.04 / 0.33±0.04	-2.61 ± 1.04
J1900–0051	136.80	1278.16 / 0.56±0.04	1336.75 / 0.46±0.03	1400.60 / 0.43±0.02	1459.61 / 0.39±0.03	-2.63 ± 0.70
J1901+0254	185.00	1277.33 / 1.22±0.06	1337.07 / 1.15±0.04	1400.04 / 1.07±0.04	1460.04 / 1.00±0.05	-1.50 ± 0.45
J1901+0413	352.00	1278.75 / 1.21±0.06	1337.08 / 1.21±0.04	1400.29 / 1.05±0.03	1459.72 / 0.98±0.04	-1.94 ± 0.44
J1902+0615	502.90	1278.75 / 2.22±0.03	1336.91 / 1.82±0.02	1400.29 / 1.62±0.02	1459.32 / 1.43±0.02	-3.27 ± 0.15
J1904+0800	438.80	1278.31 / 0.50±0.05	1336.91 / 0.47±0.03	1400.03 / 0.47±0.03	1460.04 / 0.45±0.04	-0.61 ± 0.83
J1904+1011	135.00	1277.44 / 0.54±0.04	1336.75 / 0.55±0.03	1400.45 / 0.47±0.03	1459.61 / 0.46±0.03	-1.65 ± 0.69
J1904–1224	118.23	1277.53 / 0.43±0.03	1336.91 / 0.35±0.02	1400.20 / 0.29±0.01	1460.04 / 0.25±0.02	-4.09 ± 0.63
J1905–0056	229.13	1278.75 / 0.95±0.03	1336.75 / 0.83±0.02	1400.29 / 0.71±0.02	1459.52 / 0.69±0.02	-2.64 ± 0.30
J1905+0600	730.10	1276.98 / 0.64±0.06	1336.91 / 0.53±0.04	1400.04 / 0.42±0.03	1460.04 / 0.43±0.04	-3.40 ± 0.84
J1905+0616	256.05	1275.37 / 0.61±0.04	1337.07 / 0.52±0.03	1400.04 / 0.42±0.02	1460.04 / 0.42±0.03	-3.17 ± 0.62
J1905+0709	245.34	1278.50 / 2.44±0.05	1336.75 / 2.04±0.04	1400.45 / 1.84±0.03	1459.11 / 1.75±0.04	-2.58 ± 0.20
J1906+0641	472.80	1278.75 / 3.63±0.06	1336.75 / 3.35±0.05	1400.29 / 3.26±0.04	1459.32 / 3.13±0.05	-1.03 ± 0.16
J1907+0249	261.00	1276.88 / 0.56±0.05	1336.91 / 0.46±0.03	1400.04 / 0.44±0.03	1460.04 / 0.41±0.04	-2.25 ± 0.80
J1907+0740	332.00	1276.80 / 0.77±0.04	1336.75 / 0.62±0.03	1400.45 / 0.63±0.02	1459.61 / 0.57±0.03	-1.79 ± 0.49
J1908+0457	360.00	1278.75 / 1.33±0.04	1336.75 / 1.15±0.03	1400.29 / 1.06±0.02	1459.32 / 0.89±0.03	-2.80 ± 0.29
J1908+0500	201.42	1278.75 / 1.63±0.04	1336.75 / 1.37±0.03	1400.29 / 1.29±0.03	1459.32 / 1.17±0.03	-2.37 ± 0.24
J1909+0254	171.73	1278.75 / 1.20±0.03	1336.75 / 1.07±0.02	1400.29 / 1.00±0.02	1459.32 / 0.86±0.02	-2.36 ± 0.25
J1910+0225	209.00	1277.39 / 1.14±0.05	1337.07 / 1.03±0.03	1400.04 / 0.85±0.03	1460.04 / 0.79±0.03	-2.99 ± 0.38
J1910+0714	124.06	1277.40 / 0.53±0.04	1336.91 / 0.46±0.02	1399.87 / 0.42±0.02	1460.04 / 0.37±0.03	-2.53 ± 0.66
J1913+0446	109.10	1342.75 / 0.99±0.03	1400.04 / 0.91±0.03	1465.60 / 0.86±0.03	1518.49 / 0.76±0.04	-1.84 ± 0.41
J1913+1000	422.00	1275.66 / 0.71±0.04	1337.07 / 0.65±0.02	1400.04 / 0.64±0.02	1460.04 / 0.56±0.03	-1.53 ± 0.47
J1913+1011	178.80	1342.75 / 0.59±0.04	1400.18 / 0.52±0.04	1465.60 / 0.50±0.03	1516.38 / 0.42±0.04	-2.20 ± 0.87
J1913+1145	637.00	1275.55 / 0.63±0.05	1336.91 / 0.55±0.03	1399.87 / 0.53±0.03	1460.04 / 0.48±0.03	-1.77 ± 0.68
J1914+0219	233.80	1276.45 / 1.74±0.04	1337.61 / 1.57±0.03	1400.04 / 1.53±0.03	1460.04 / 1.47±0.03	-1.14 ± 0.22
J1915+0227	192.60	1277.24 / 0.58±0.04	1337.07 / 0.40±0.03	1400.04 / 0.40±0.02	1460.04 / 0.36±0.03	-3.18 ± 0.76
J1915+1606	168.77	1277.11 / 1.26±0.05	1337.07 / 1.00±0.03	1400.04 / 0.85±0.03	1460.04 / 0.83±0.03	-3.23 ± 0.39
J1916+0844	339.40	1342.75 / 0.63±0.03	1399.76 / 0.61±0.02	1465.60 / 0.57±0.02	1513.92 / 0.54±0.03	-1.28 ± 0.51
J1916+1023	329.80	1277.71 / 0.93±0.09	1336.91 / 0.80±0.06	1399.87 / 0.76±0.05	1460.04 / 0.74±0.06	-1.62 ± 0.86
J1917+2224	134.93	1277.25 / 0.45±0.04	1337.24 / 0.42±0.03	1400.03 / 0.36±0.03	1460.04 / 0.35±0.03	-2.22 ± 0.80
J1920+1040	304.00	1277.23 / 1.28±0.10	1336.91 / 1.12±0.06	1400.04 / 0.96±0.06	1460.04 / 0.82±0.07	-3.37 ± 0.79
J1927+1856	99.00	1276.60 / 0.72±0.05	1336.91 / 0.56±0.03	1399.87 / 0.55±0.03	1460.04 / 0.49±0.04	-2.52 ± 0.70
J1935+1745	214.60	1277.12 / 0.20±0.02	1336.91 / 0.18±0.01	1400.04 / 0.16±0.01	1460.04 / 0.13±0.02	-3.04 ± 1.12

the profile components would not disappear quickly. The disadvantage is that the uncertainty associated with such a determined spectral index is large due to the limited frequency range. The best spectral measurements in the future would be made for each profile component within one ultra wide band. The weak correlations between spectral indexes and $\dot{E}$ and $\Delta\Psi$ imply that the radiation properties are physically related to the particle acceleration process.

Table 3 Comparison of spectral indexes of 28 pulsars that we determined with those in literature.

Pulsar Name	Our α	Other α	Frequency (MHz)	Reference
J1744–3130	-1.66 ± 0.41	-1.1	610–1170	Dembska et al. 2014
J1751–3323	-1.53 ± 0.24	-0.32	610–1170	Dembska et al. 2014
J1812–2102	-1.00 ± 0.33	-2 ± 0.1	610–4850	Dembska et al. 2014
J1835–1020	-1.22 ± 0.17	-0.8	610–1170	Dembska et al. 2014
J1842–0905	-2.22 ± 0.30	-1.2	610–1170	Dembska et al. 2014
J1905+0616	-3.17 ± 0.62	-0.88 ± 0.25	610–4850	Dembska et al. 2014
J1644–4559	-2.90 ± 0.00	-2.1 ± 0.1	1400–6500	Bates et al. 2011
J1707–4053	-2.99 ± 0.20	-2.3 ± 0.1	1400–6500	Bates et al. 2011
J1804–0735	-2.35 ± 0.67	-1.3 ± 0.31	400–1400	Maron et al. 2000
J1816–1729	-1.97 ± 0.26	-1 ± 0.14	600–1600	Maron et al. 2000
J1818–1422	-2.46 ± 0.14	-1.6 ± 0.22	900–1600	Maron et al. 2000
J1822–1400	-2.25 ± 0.43	-0.7 ± 0.22	600–1400	Maron et al. 2000
J1832–1021	-2.93 ± 0.22	-1.3 ± 0.15	400–1600	Maron et al. 2000
J1835–0643	-2.01 ± 0.47	-0.4 ± 0.35	600–1600	Maron et al. 2000
J1836–1008	-2.98 ± 0.14	-2.1 ± 0.09	400–1600	Maron et al. 2000
J1836–0436	-1.85 ± 0.18	-1.9 ± 0.3	600–1600	Maron et al. 2000
J1837–0653	-1.58 ± 0.16	-1.2 ± 0.24	600–1600	Maron et al. 2000
J1845–0434	-1.18 ± 0.24	-0.8 ± 0.29	600–1400	Maron et al. 2000
J1852+0031	-1.12 ± 0.19	-2.4 ± 0.12	1400–4900	Maron et al. 2000
J1851+0418	-2.09 ± 0.29	-1.4	600–1400	Maron et al. 2000
J1902+0615	-3.27 ± 0.15	-2.2 ± 0.1	400–4900	Maron et al. 2000
J1905–0056	-2.64 ± 0.30	-1.9 ± 0.11	400–1400	Maron et al. 2000
J1905+0709	-2.58 ± 0.20	-1.3 ± 0.1	600–1400	Maron et al. 2000
J1906+0641	-1.03 ± 0.16	-0.7 ± 0.21	400–1600	Maron et al. 2000
J1909+0254	-2.36 ± 0.25	-2.8 ± 0.11	400–1400	Maron et al. 2000
J1915+1606	-3.23 ± 0.39	-1.4 ± 0.24	400–1400	Maron et al. 2000
J0738–4042	-1.89 ± 0.01	-0.69	400–1400	Slee et al. 1986
J0952–3839	-4.27 ± 0.54	-1.96	160–400	Slee et al. 1986

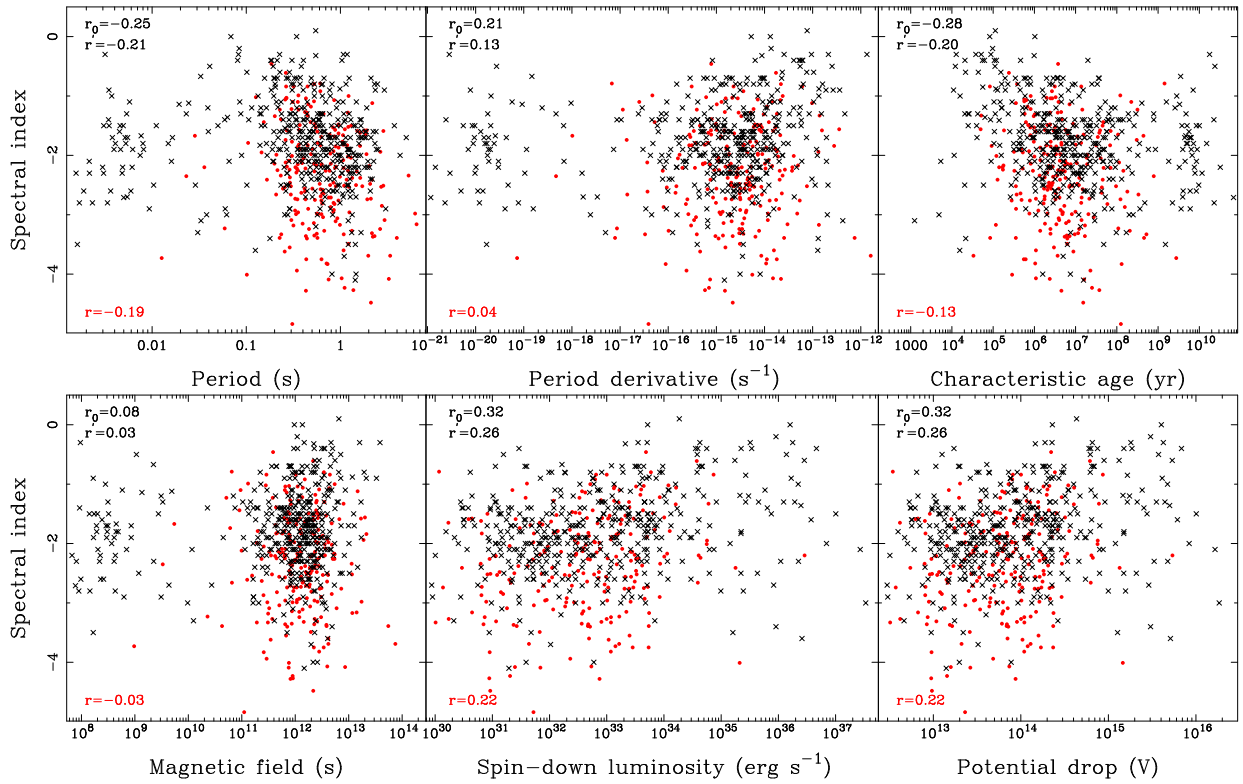

Fig. 3 Spectral indices that we determined (*dots*) and those in literature (*crosses*) are plotted against pulsar characteristic parameters: period P, period derivative $\dot{P}$, age τ, surface magnetic field B, spin-down luminosity $\dot{E}$, and polar gap potential drop $\Delta\Psi$. The Spearman rank correlation parameters are marked for normal pulsars in literature (r_0) and in our sample (r) as well as the combined sample (r').

Table 4 The Spearman rank correlation parameters for spectral indices versus P, τ, $\dot{P}$, B, $\dot{E}$ and $\Delta\Psi$ for 372 normal pulsars in literatures (r_0) and 224 normal pulsars (excluding 4 millisecond pulsars) in our sample (r) as well as 572 pulsars in the combined sample (r').

	α vs. P	α vs. $\dot{P}$	α vs. τ	α vs. B	α vs. $\dot{E}$	α vs. $\Delta\Psi$
372 pulsars (r_0)	-0.25	0.21	-0.28	0.08	0.32	0.32
224 pulsars (r)	-0.19	0.04	-0.13	-0.03	0.22	0.22
572 pulsars (r')	-0.21	0.13	-0.20	0.03	0.26	0.26

Acknowledgements The authors are supported by the National Natural Science Foundation of China (No. 11473034) and by the Strategic Priority Research Program "The Emergence of Cosmological Structures" of the Chinese Academy of Sciences, Grant No. XDB09010200.

References

Bates, S. D., Johnston, S., Lorimer, D. R., et al. 2011, MNRAS, 411, 1575
Cordes, J. M. 1978, ApJ, 222, 1006
Dembska, M., Kijak, J., Jessner, A., et al. 2014, MNRAS, 445, 3105
Deneva, J. S., Cordes, J. M., & Lazio, T. J. W. 2009, ApJ, 702, L177
Foster, R. S., Fairhead, L., & Backer, D. C. 1991, ApJ, 378, 687
Hewish, A., Bell, S. J., Pilkington, J. D. H., Scott, P. F., & Collins, R. A. 1968, Nature, 217, 709
Hobbs, G., Miller, D., Manchester, R. N., et al. 2011, PASA, 28, 202
Izvekova, V. A., Kuzmin, A. D., Malofeev, V. M., & Shitov, I. P. 1979, AZh, 56, 322
Joshi, B. C., McLaughlin, M. A., Lyne, A. G., et al. 2009, MNRAS, 398, 943
Kijak, J., Kramer, M., Wielebinski, R., & Jessner, A. 1998, A&AS, 127, 153
Komesaroff, M. M. 1970, Nature, 225, 612
Kramer, M., Lange, C., Lorimer, D. R., et al. 1999, ApJ, 526, 957
Kramer, M., Xilouris, K. M., Lorimer, D. R., et al. 1998, ApJ, 501, 270
Lambert, H. C., & Rickett, B. J. 1999, ApJ, 517, 299
Lommen, A. N., Zepka, A., Backer, D. C., et al. 2000, ApJ, 545, 1007
Lorimer, D. R., & Xilouris, K. M. 2000, ApJ, 545, 385
Lorimer, D. R., Yates, J. A., Lyne, A. G., & Gould, D. M. 1995, MNRAS, 273, 411
Malofeev, V. M. 1996, in Astronomical Society of the Pacific Conference Series, 105, IAU Colloq. 160: Pulsars: Problems and Progress, ed. S. Johnston, M. A. Walker, & M. Bailes, 271
Malofeev, V. M., Gil, J. A., Jessner, A., et al. 1994, A&A, 285, 201
Malofeev, V. M., Malov, O. I., & Shchegoleva, N. V. 2000, Astronomy Reports, 44, 436
Maron, O., Kijak, J., Kramer, M., & Wielebinski, R. 2000, A&AS, 147, 195
McLaughlin, M. A., Arzoumanian, Z., Cordes, J. M., et al. 2002, ApJ, 564, 333
Melrose, D. B. 2006, Chinese Journal of Astronomy and Astrophysics Supplement, 6, 74
Moffett, D. A., & Hankins, T. H. 1996, ApJ, 468, 779
Press, W. H., Teukolsky, S. A., Vetterling, W. T., & Flannery, B. P. 1992, Numerical Recipes in FORTRAN. The Art of Scientific Computing (2nd edn.; Cambridge: Cambridge University Press)
Radhakrishnan, V., & Cooke, D. J. 1969, Astrophys. Lett., 3, 225
Rankin, J. M. 1983, ApJ, 274, 333
Rankin, J. M., Comella, J. M., Craft, Jr., H. D., et al. 1970, ApJ, 162, 707
Robinson, B. J., Cooper, B. F. C., Gardiner, F. F., Wielebinski, R., & Landecker, T. L. 1968, Nature, 218, 1143
Sieber, W. 1973, A&A, 28, 237
Sieber, W., Reinecke, R., & Wielebinski, R. 1975, A&A, 38, 169
Slee, O. B., Alurkar, S. K., & Bobra, A. D. 1986, Australian Journal of Physics, 39, 103
Toscano, M., Bailes, M., Manchester, R. N., & Sandhu, J. S. 1998, ApJ, 506, 863